JACS
JOURNAL OF THE AMERICAN CHEMICAL SOCIETY
Article
Cite This: J. Am. Chem. Soc. 2019, 141, 14807−14813
pubs.acs.org/JACS

Three Models To Encapsulate Multicomponent Dyes into Nanocrystal Pores: A New Strategy for Generating High-Quality White Light

Xiao-Yuan Liu,[†,‡] Kai Xing,[‡] Yang Li,[§] Chia-Kuang Tsung,*[,§] and Jing Li*[,‡,†]

[†]Hoffmann Institute of Advanced Materials, Shenzhen Polytechnic, 7098 Liuxian Boulevard, Nanshan District, Shenzhen 518055, P.R. China

[‡]Department of Chemistry and Chemical Biology, Rutgers University, 123 Bevier Road, Piscataway, New Jersey 08854, United States

[§]Department of Chemistry, Merkert Chemistry Center, Boston College, 2609 Beacon Street, Chestnut Hill, Massachusetts 02467, United States

Supporting Information

ABSTRACT: Highly luminescent metal−organic frameworks (LMOFs) have received great attention for their potential use in energy-efficient general lighting devices such as white-light-emitting diodes (WLEDs); however, achieving strong emission with controllable color, especially high-quality white light, remains a considerable challenge. Herein, we present a new strategy to encapsulate in situ multiple dyes into nanocrystalline ZIF-8 pores to form an efficient dyes@MOF system. Using this strategy, we build three models, namely, multiphase single-shell dye@ZIF-8, single-phase single-shell dyes@ZIF-8, and single-phase multishell dyes@ZIF-8, to systematically and fine-tune the white emission color by varying the components and concentration of encapsulated dyes. The study of these three models demonstrates the importance of the multishell structure, which can effectively reduce the interactions such as Förster resonance energy transfer (FRET) between encapsulated dyes. This energy transfer would otherwise be unavoidable in a single-shell setting, which often reduces the efficiency of white-light emission in the dyes@MOF system. This approach offers a new perspective not only for fine-tuning the emission color within nanoporous dyes@MOFs but also for fabricating MOF nanocrystals that are easily solution-processable. The strategy may also facilitate the development of other types of MOF−guest nanocomposite systems.

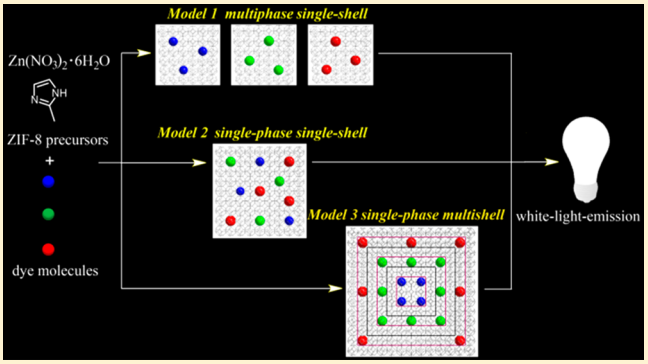

INTRODUCTION

Since the first report on metal−organic framework (MOF)-based white light emission (WLE) in 2009,[1] many efforts have been made to improve the WLE performance via changing the MOF structure and composition.[2−5] So far, WLE has been generated on the basis of four types of emission sources: (1) organic ligands,[6−10] (2) metal nodes or metal nodes combined with ligands,[11−13] (3) encapsulated guest species,[14−18] and (4) organic ligands combined with guest materials.[19] Among these categories, MOF-guest-based systems show some advantages over others, where neither metal centers nor ligands are required to be emissive so that the selection of MOFs is expanded. In these systems, MOFs serve as a scaffold for the dye guests to prevent aggregation-caused quenching (ACQ). Typically, the MOF−guest composites are synthesized using a two-step process, where a pristine MOF is synthesized first and then selected dyes are incorporated into MOFs via ion exchange.[14,15,20−22] These dyes@MOF composites often exhibit great WLE performance; however, this approach has certain limitations. For example, the size of the dyes must be small enough to fit into the aperture of the MOF pores. Also, the leakage of the dye molecules is another issue if the host−guest interactions are not sufficiently strong. In addition, the interaction between different dyes, such as fluorescence resonance energy transfer (FRET), could interfere with the WLE and reduce its efficiency.

A recent study shows that if different dye molecules are encapsulated into MOF at different locations, then bright WLE with a CIE (0.35, 0.32) could be achieved.[16] Control of the guest location in this work is achieved via a core−shell cyclodextrin-based MOF, in which the time-consuming synthesis and the microsized crystal could limit the device fabrication and commercial applications. As such, further improvements in developing dyes@MOF-based systems with a

Received: July 8, 2019
Published: August 19, 2019

Downloaded via RUTGERS UNIV on September 18, 2019 at 12:10:42 (UTC).
See https://pubs.acs.org/sharingguidelines for options on how to legitimately share published articles.

© 2019 American Chemical Society

DOI: 10.1021/jacs.9b07236
J. Am. Chem. Soc. 2019, 141, 14807−14813

facile synthesis route, high processability, and excellent WLE performance are much needed.

Herein, we present a facile approach to encapsulating multiple dyes into zeolitic imidazolate framework 8 (ZIF-8) during crystal formation. To understand and control the effect of dye locations on WLE, three models are established, namely, multiphase single-shell dye@ZIF-8 (model 1), single-phase single-shell dyes@ZIF-8 (model 2), and single-phase multishell dyes@ZIF-8 (model 3) (Scheme 1).[23] We hypothesize that the

Scheme 1. Schematic Diagrams of Three Models for the Preparation of Dye and ZIF-8-Based Composites for White Light Emission

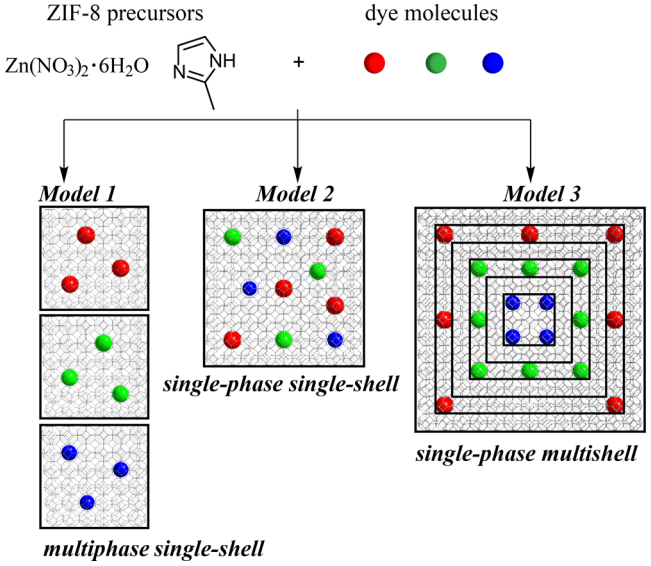

WLE can be achieved in all three models by changing the components and concentrations of dyes molecules, and the multishell structure in model 3 can eliminate the interactions between different dye molecules by placing them in different shells, which represents an entirely new design.[24,25] The reasons for choosing ZIF-8 as the host MOF are threefold: (1) ZIF-8 can be easily synthesized in water and organic solvent at room temperature, which allows a broader selection of dyes;[26,27] (2) the size control and shape control of ZIF-8 nanocrystals are reported, which allows us to have desirable nanocrystals for the solution-based fabrication of WLE devices; and (3) the encapsulation of multiple guest species inside the ZIF-8 with controlled locations has been established.[23,28]

RESULTS AND DISCUSSION

To demonstrate our proof-of-concept design, three dye molecules were chosen as encapsulates. They emit three different colors, namely, red (rhodamine B or RB), green (fluorescein or F), and blue (7-amino-4-(trifluoromethyl)-coumarin or C-151). A careful analysis was made to ensure a good match between the ZIF-8 pore structure and the dimensions of these dye molecules. As shown in Figure 1, the aperture of the pore window and the cage size of ZIF-8 are 3.40 and 11.6 Å,[29] respectively. Therefore, the selected dyes should be larger than the aperture size but on a length scale similar to that of the cavity in order to be securely encapsulated within the ZIF-8 pores. The molecular sizes of RB, F, and C-151 are ~10.2 × 16.8, 11.0 × 13.0, and 8.0 × 11.0 Å (Figure 1b–d),[30,31] respectively, matching the requirement well.

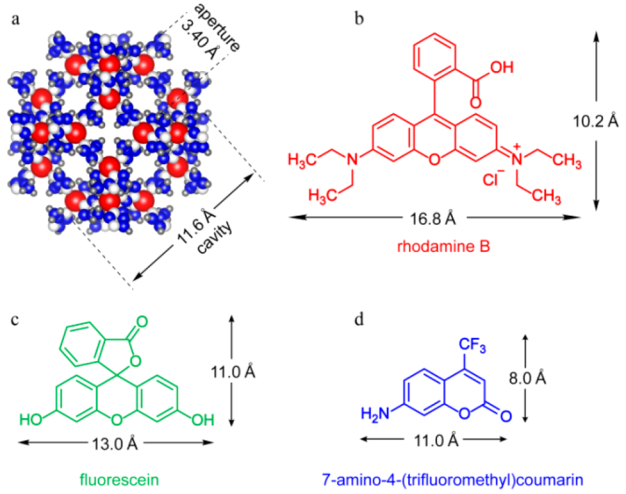

Figure 1. (a) Single-crystal structure of ZIF-8, where the aperture and cage sizes are indicated. (b–d) Chemical structures and molecular dimensions of rhodamine B (RB), fluorescein (F), and 7-amino-4-(trifluoromethyl)coumarin (C-151).

Then we first applied model 1 to synthesize multiphase single-shell dye@ZIF-8 to demonstrate that ZIF-8 is capable of trapping different kinds of dyes in situ.[32] A designated amount of each dye was added to a ZIF-8 precursor solution and reacted at room temperature. The formed dye@ZIF-8 nanocrystals were washed thoroughly using methanol. The fluorescence spectra show that the emission profiles of all three dye-encapsulated ZIF-8 nanocrystals resemble those of the pristine dyes (Figure S1), with only a slight shift in the emission maximum. Methanol solutions of C-151@ZIF-8, F@ZIF-8, and RB@ZIF-8 show blue, green, and red emission, respectively (Figure S1). To rule out the effect on the composite emission from the surface-absorbed dyes, the water–methanol-mediated overgrowth method was used to coat a pure ZIF-8 shell on the dye@ZIF-8 nanocrystals to obtain dye@ZIF-8@ZIF-8 (dye@ZIF-8^2).[23] The concentration of each dye was then varied to investigate its effect on the emission properties of dye@ZIF-8^2 nanocomposites. As shown in Figure 2a–c, the fluorescence intensity of dye@ZIF-8^2 increases initially with increasing concentration of encapsulated dyes (Figures S2–S4, Tables S1–S3). Further increases in concentration lead to an intensity drop. For F@ZIF-8^2 and RB@ZIF-8^2, a red shift in emission energy is observed with increasing dye concentration. The quantum yields (QYs) follow the same trend as the emission intensity (Tables S1–S3). The gradual color changes of solid C-151@ZIF-8^2, F@ZIF-8^2, and RB@ZIF-8^2 under daylight and UV light also indicate the successful encapsulation of C-151, F, and RB into ZIF-8 with increasing concentration. The highest QYs are 0.419 for C-151@ZIF-8^2, 0.626 for F@ZIF-8^2, and 0.601 for RB@ZIF-8^2 with contents of 0.0137, 0.0072, and 0.0372 wt %, respectively. Increases of 47-, 125-, and 20-fold are compared to those of the pristine dye molecules in their solid states (0.009, 0.005, and 0.03 for C-151, F, and RB, respectively). These results reveal that dye@ZIF-8^2 nanocomposites can effectively reduce the aggregation-caused quenching (ACQ) by confining and isolating the dye molecules within individual ZIF-8 pores[33,34] and that the in situ encapsulation approach is a powerful method for traping different dyes in the ZIF-8 pore space during crystal formation to achieve higher QY in the solid state. The best obtained CIE coordinates are (0.16, 0.12),

DOI: 10.1021/jacs.9b07236
J. Am. Chem. Soc. 2019, 141, 14807–14813

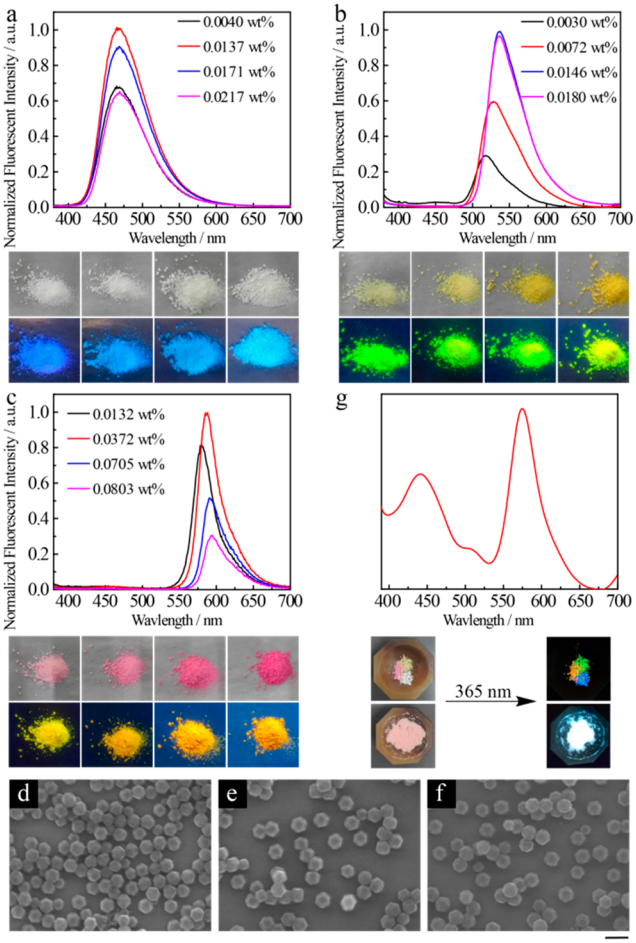

Figure 2. Liquid-state fluorescence spectra of (a) C-151@ZIF-8^2, (b) F@ZIF-8^2, and (c) RB@ZIF-8^2 nanocrystals with different dye concentrations in methanol solution under 365 nm excitation and photographs of corresponding composites under daylight (top) and UV light (bottom). (d–f) SEM images of C-151@ZIF-8^2, F@ZIF-8^2, and RB@ZIF-8^2 nanocrystals, with a scale bar of 200 nm. (g) The solid-state fluorescence spectrum of a composite of C-151@ZIF-8^2, F@ZIF-8^2, and RB@ZIF-8^2 (2:1:3 for 0.0137 wt % C-151@ZIF-8^2/0.0146 wt % F@ZIF-8^2/0.0372 wt % RB@ZIF-8^2) and the corresponding photographs without (top) or with (bottom) grinding under daylight (left) and UV light (right).

(0.26, 0.58), and (0.57, 0.43) for C-151@ZIF-8^2, F@ZIF-8^2, and RB@ZIF-8^2 respectively (Figure S5), which are close to the saturated blue (0.14, 0.08), green (0.21, 0.71), and red (0.66, 0.33) emitters. The structure of dye@ZIF-8^2 nanocrystals was characterized by scanning electron microscopy (SEM) and powder X-ray diffraction (PXRD) methods. As shown in Figure 2d–f, uniform truncated rhombic dodecahedrons were obtained for all dye@ZIF-8^2 composites. PXRD patterns of dye@ZIF-8^2 nanocomposite samples with different concentrations are identical to that of the simulated PXRD pattern of ZIF-8 (Figure S6).[35] These data confirm that the introduction of dye molecules into the ZIF-8 cavity does not alter its crystal structure

The excellent emission properties of C-151@ZIF-8^2, F@ZIF-8^2, and RB@ZIF-8^2 prompted us to evaluate the possibility of combining the three colors to achieve WLE by simply mixing these three composites. As expected, the WLE was realized by optimizing the ratio of C-151@ZIF-8^2, F@ZIF-8^2, and RB@ZIF-8^2. For example, when a mixture of 0.0137 wt % C-151@ZIF-8^2, 0.0146 wt % F@ZIF-8^2, and 0.0372 wt % RB@ZIF-8^2 with a mass ratio of 2:1:3 was ground, a WLE was indeed achieved as shown in Figure 2g. The corresponding CIE coordinates of (0.32, 0.34) were calculated (Figure S5), which are very close to the pure white color of (0.33, 0.33). These results indicate that single-shell dye@ZIF-8^2 nanocrystals can be combined to form multiphase phosphors of targeted colors. In addition, because of the nanosize of dye@ZIF-8^2, they can be well dispersed in solution, making them highly solution-processable for device fabrication (Figure S7).

The above results inspired us to explore model 2 (Scheme 1). Would the encapsulation of red, green, and blue emitting dyes simultaneously in ZIF-8 lead to a single-phase C-151&F&RB@ZIF-8^2, for which the WLE color may be tuned and optimized by adjusting the concentrations of encapsulated C-151, F, and RB? Also, by combining all of the dyes in one nanocrystal, we can optimize the emission property in a more direct way and simplify the fabrication process. To answer this question, we applied model 2 to synthesize a single-phase, single-shell C-151&F&RB@ZIF-8^2 composite by adding C-151, F, and RB simultaneous to precursor solutions of ZIF-8. As expected, by carefully adjusting the concentration of three dyes, white emitting C-151&F&RB@ZIF-8^2 composites were obtained. For example, using 20 μL of 5 mM C-151, 40 μL of 5 mM F, and 20 μL of 5 mM RB (Figure 3a, black line) or 20 μL

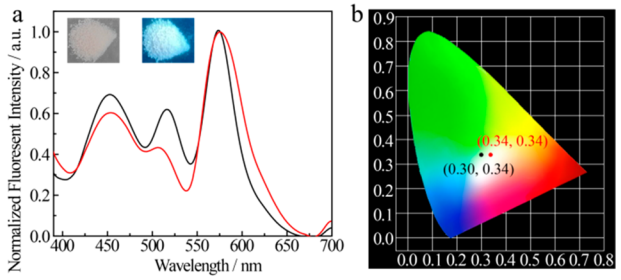

Figure 3. (a) Solid-state fluorescence spectra of C-151&F&RB@ZIF-8^2 with different concentrations of dyes under the excitation of 365 nm (inset: a C-151&F&RB@ZIF-8^2 sample under daylight and UV light) and (b) the corresponding CIE chromaticity coordinates.

of 5 mM C-151, 20 μL of 5 mM F, and 40 μL of 5 mM RB (Figure 3a, red line) for the synthesis, both nanocrystals led to emission spectra that cover the visible light region (400–650 nm) with WLE. The corresponding CIE chromaticity coordinates, (0.30, 0.34) and (0.34, 0.34), are both very close to pure white light (Figure 3b), which demonstrates that model 2 can also be employed as a strategy to realize WLE by combing three dyes together under optimized conditions. However, because of the strong fluorescence resonance energy transfer (FRET) among these three dyes (Figure S8), it is difficult to calculate their accurate concentrations upon mixing them together.

As mentioned above, one major drawback of model 2 is the energy transfer among the emissive dye molecules, which cannot be ignored because the efficiency of WLE might be significantly decreased by these kinds of interactions. For C-151, F, and RB, strong FRET was found in their binary mixture solutions (Figure S8). To avoid this, we propose to place different dyes at different locations (shells) on a nanocrystal. It was found in a previous study that it is possible to encapsulate different guest molecules into a multishell ZIF-8 nanocrystal with sufficiently large spatial separation, in which the FRET

DOI: 10.1021/jacs.9b07236
J. Am. Chem. Soc. 2019, 141, 14807–14813

between two guests can be totally suppressed by the solid ZIF-8 shell.[23] Therefore, we developed model 3, a single-phase multishell dyes@ZIF-8^2 (Scheme 1) where the three dyes are encapsulated consecutively into ZIF-8 nanocrystals via shell-by-shell overgrowth and separated by solid ZIF-8 shells. As shown in Figure 4a, the first step is to encapsulate two dyes (in any combination) into multishell ZIF-8 during crystal formation, where the emission color of multishell dyes@ZIF-8^2 can be easily tuned from pink to yellow to cyan by the formation of RB@ZIF-8^2@C-151@ZIF-8^2, RB@ZIF-8^2@F@ZIF-8^2, and C-151@ZIF-8^2@F@ZIF-8^2, respectively. As one example to confirm our hypothesis, C-151@ZIF-8^2 was used as the core to perform the overgrowth of F@ZIF-8 with increased F concentrations, and the thus-formed C-151@ZIF-8^2@F@ZIF-8^2 was then used as the new core for further overgrowth of RB@ZIF-8 to prepare the multishell dyes@ZIF-8^2 nanocomposites for WLE (Figure S9 and Figure 4b).

As shown in Figure 4b,c, under the optimized synthesis conditions, the CIE chromaticity coordinates of multishell C-151@ZIF-8^2@F@ZIF-8^2@RB@ZIF-8^2 changed from (0.21, 0.26) to (0.32, 0.34) with increasing RB concentration, suggesting that model 3 can also be very efficient for preparing composite materials with systematically tunable emission colors, including white light. The multishell structure formation was further proven with a scanning electron microscope (SEM) as depicted in Figure 4d. Via sequential shell-by-shell overgrowth in water and methanol, it is observed that the size of ZIF-8 gradually increased, accompanied by the morphology switch between a truncated cube and a truncated rhombic dodecahedron. The growth sequence and the thickness of the shells did not have an obvious effect on the light quality. The emission spectrum and CIE chromaticity coordinates of the white-light-emitting RB@ZIF-8^2@F@ZIF-8^2@C-151@ZIF-8^2 multishell nanocomposite (Figure S10a) are very similar to those of C-151@ZIF-8^2@F@ZIF-8^2@RB@ZIF-8^2 (Figure 4b). In addition, very small changes were observed in the fluorescence of RB@ZIF-8^2@F@ZIF-8^2@C-151@ZIF-8^2 samples with a different outer-shell thickness of ZIF-8 (Figure S10b).

The PXRD patterns of single-phase single-shell dye@ZIF-8^2, multiphase single-shell dyes@ZIF-8^2, and single-phase multishell dyes@ZIF-8^2 remain essentially the same as that of the simulated ZIF-8 (Figure 4e), confirming that the in situ encapsulated dyes have no effect on the single-crystal structure of the pristine ZIF-8. Leak-checking experiments confirmed that the dyes were well trapped within the ZIF-8 pores. All samples tested showed no trace of leakage (Figure S11).

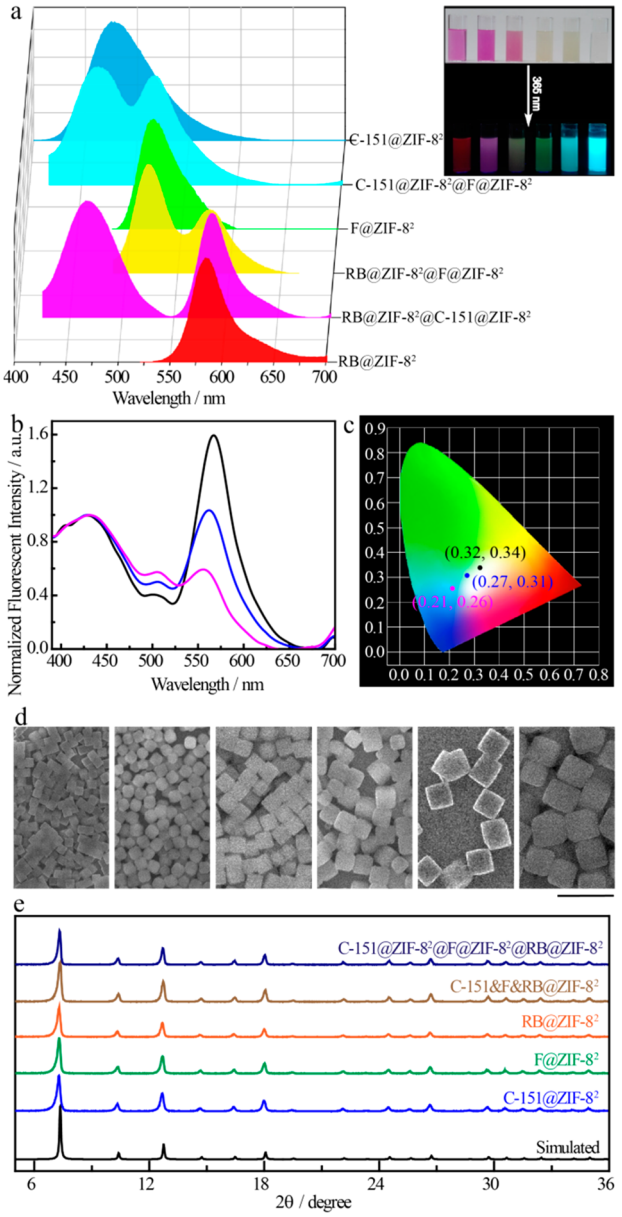

Figure 4. (a) Liquid-state fluorescence spectra of single-shell dye@ZIF-8^2 and double-shell dyes@ZIF-8^2 in methanol solution under 365 nm excitation and their corresponding photographs under daylight and UV light (RB@ZIF-8^2 to C-151@ZIF-8^2 from left to right). (b) Solid-state fluorescence spectra and (c) the corresponding CIE chromaticity coordinates of C-151@ZIF-8^2@F@ZIF-8^2@RB@ZIF-8^2 with different concentrations of RB (200 μL of 0.5 mM C-151, 200 μL of 5 mM F, and 10, 20, and 100 μL of 0.5 mM RB for pink, blue, and black lines, respectively). (d) SEM images of various nanocrystal samples, from left to right: C-151@ZIF-8, C-151@ZIF-8^2, C-151@ZIF-8^2@F@ZIF-8, C-151@ZIF-8^2@F@ZIF-8^2, C-151@ZIF-8^2@F@ZIF-8^2@RB@ZIF-8, and C-151@ZIF-8^2@F@ZIF-8^2@RB@ZIF-8^2, scale bar 1 μm. (e) PXRD patterns of simulated ZIF-8, C-151@ZIF-8^2, F@ZIF-8^2, RB@ZIF-8^2, C-151&F&RB@ZIF-8^2, and C-151@ZIF-8^2@F@ZIF-8^2@RB@ZIF-8^2.

CONCLUSIONS

We have developed a facile approach to preparing dyes@MOF-based host−guest nanocomposites to generate white light emission via the in situ encapsulation of dyes into ZIF-8 pores during its crystal formation. We have studied three models in which the dye locations are tunable. To avoid an energy-transfer-caused efficiency decrease due to the interactions between encapsulated dye molecules, a single-phase multishell dyes@ZIF-8 nanocomposite could confine and isolate different dye molecules in different ZIF-8 shells. By adjusting the composition and concentration of encapsulated dyes, the dyes@ZIF-8 composites prepared on the basis of the three models all show high WLE quality. Combining the facile and scalable synthesis, the use of inexpensive and commercially available dyes, and systematic color tunability, this study has offered a novel and efficient approach to making highly solution-processable dyes@MOFs-based nanocomposite materials that are promising candidate for use as a new family of phosphors in energy-efficient lighting devices.

DOI: 10.1021/jacs.9b07236
J. Am. Chem. Soc. 2019, 141, 14807−14813

EXPERIMENTAL SECTION

General Information. The commercial chemicals were used without further purification, and a detailed list of chemicals can be found in the Supporting Information.

Instruments. The fluorescence spectra were measured using a Fluoromax-4 spectrofluorometer from Horiba Scientific. The quantum yield was obtained using a C11347 absolute PL quantum yield spectrometer. Powder X-ray diffraction patterns were measured using an Ultima IV X-ray diffractometer with Cu Kα radiation. Scanning electron microscope (SEM) images were obtained on a JEOL JSM6340F.

Synthesis of dye@ZIF-8. The dye@ZIF-8 was synthesized using two different methods (A and B), where method A has a much higher yield than method B but method B has better morphology and size control than method A for the synthesis of multishell ZIF-8.

Synthesis of ZIF-8 (Method A). A 5 mL aqueous solution containing 2.72 M 2-methylimidazole and 0.55 mM CTAB was stirred for 1 min, followed by the addition of 5 mL of a 300 mg $Zn(CH_3COO)_2{\cdot}2H_2O$ aqueous solution. The mixture was stirred for another 10 s and then was left undisturbed for 2 h at room temperature. The synthesized R6G@ZIF-8 was spun down at 9000 rpm for 10 min and washed twice using methanol.[32]

Synthesis of C-151@ZIF-8 (0.0040, 0.0137, 0.0171, and 0.0217 wt %) (Method A). A 5 mL aqueous solution containing 2.72 M 2-methylimidazole and 0.55 mM CTAB was stirred for 1 min, followed by the addition of 5 mL of a 300 mg $Zn(CH_3COO)_2{\cdot}2H_2O$ aqueous solution. After the mixture was stirred for 10 s, different amounts of a 5 mM C-151 methanol solution (0.10, 0.37, 0.50, and 0.75 mL) were added. The mixture was stirred for another 10 s and then was left undisturbed for 2 h at room temperature. The synthesized R6G@ZIF-8 was spun down at 9000 rpm for 10 min and washed twice using methanol.

Synthesis of F@ZIF-8 (0.0030, 0.0072, 0.0146, and 0.0180 wt %) (Method A). A 5 mL aqueous solution containing 2.72 M 2-methylimidazole and 0.55 mM CTAB was stirred for 1 min, followed by the addition of 5 mL of 300 mg of $Zn(CH_3COO)_2{\cdot}2H_2O$ aqueous solution. After the mixture was stirred for 10 s, different amounts of 5 mM F in a solution containing 2.72 M 2-methylimidazole and 0.55 mM CTAB (0.10, 0.25, 0.75, and 1.00 mL) were added. The mixture was stirred for another 10 s and then was left undisturbed for 2 h at room temperature. The synthesized R6G@ZIF-8 was spun down at 9000 rpm for 10 min and washed twice using methanol.

Synthesis of RB@ZIF-8 (0.0132, 0.0372, 0.0705, and 0.0803 wt %) (Method A). A 5 mL aqueous solution containing 2.72 M 2-methylimidazole and 0.55 mM CTAB was stirred for 1 min, followed by the addition of 5 mL of 300 mg of a $Zn(CH_3COO)_2{\cdot}2H_2O$ aqueous solution. After the mixture was stirred for 10 s, different amounts of 5 mM RB aqueous solution (0.10, 0.25, 0.50, and 0.75 mL) were added. The mixture was stirred for another 10 s and then was left undisturbed for 2 h at room temperature. The synthesized R6G@ZIF-8 was spun down at 9000 rpm for 10 min and washed twice using methanol.

Synthesis of dye@ZIF-8@ZIF-8 (dye@ZIF-8^2). A 60 mL solution of 30 mM 2-methylimidazole was used to redisperse the as-synthesized dye@ZIF-8, and then 60 mL of a 30 mM $Zn(NO_3)_2{\cdot}6H_2O$ methanol solution was added. After being shaken for 10 s, the mixture solution was left undisturbed at room temperature for 1.5 h, and the formed dye@ZIF-8^2 was spun down at 6000 rpm for 10 min.[28]

Synthesis of C-151&F&RB@ZIF-8 (Method A). A 5 mL aqueous solution containing 2.72 M 2-methylimidazole and 0.55 mM CTAB was stirred for 1 min, followed by the addition of 5 mL of a 300 mg $Zn(CH_3COO)_2{\cdot}2H_2O$ aqueous solution. After the mixture was stirred for 10 s, a mixture solution of C-151, F, and RB was added. The mixture was stirred for another 10 s and then was left undisturbed for 2 h at room temperature. The synthesized C-151&F&R6G@ZIF-8 was spun down at 9000 rpm for 10 min and washed twice using methanol (one example for white light emission: 0.25 mL of 0.5 mM C-151, 0.1 mL of 0.5 mM F, and 0.05 mL of 0.5 mM RB).

Synthesis of C-151&F&RB@ZIF-8 (Method B). A 17.5 mL solution of 790 mM 2-methylimidazole and 0.275 mM CTAB was stirred at 800 rpm for 5 min, followed by the addition of 2.5 mL of a 97.5 mM $Zn(NO_3)_2{\cdot}6H_2O$ aqueous solution. After the mixture was stirred for 3 min, a mixture solution of C-151, F, and RB was added, and the solution continued to stir for 2 min. Then the solution was left undisturbed for 3 h at room temperature. The synthesized C-151&F&RB@ZIF-8 composites were spun down at 8000 rpm for 10 min, washed twice using methanol, and then dispersed in 5 mL of methanol (one example for white light emission: 20 μL of 5 mM C-151, 40 μL of 5 mM F, and 20 μL of 5 mM RB).

Synthesis of Rhodamine C-151&F&RB@ZIF-8^2. C-151&F&RB@ZIF-8^2 was synthesized using the same method as in the synthesis of dye@ZIF-8^2.

Synthesis of C-151@ZIF-8 (Method B). A 1.75 mL solution of 790 mM 2-methylimidazole and 0.55 mM CTAB was stirred for 5 min, followed by the addition of 0.25 mL of a 97.5 mM $Zn(NO_3)_2{\cdot}6H_2O$ aqueous solution. After the mixture was stirred for 3 min, 0.2 mL of a 0.5 mM C-151 methanol solution was added and the mixture continued to stir for 2 min. Then the solution was left undisturbed for 3 h at room temperature. The synthesized C-151@ZIF-8 composites were spun down at 8000 rpm for 10 min, washed twice using methanol, and then dispersed in methanol.[28]

F@ZIF-8 and RB@ZIF-8 were synthesized using the same method as for C-151@ZIF-8.

Synthesis of C-151@ZIF-8^2. An as-synthesized C-151@ZIF-8 composite was added into 15 mL of a methanol solution containing 30 mM 2-methylimidazole. After the solution was shaken for 5 s, 15 mL of a 30 mM $Zn(NO_3)_2{\cdot}6H_2O$ methanol solution was added. Then the solution was left undisturbed at room temperature for 1 h, and the formed C-151@ZIF-8^2 was spun down at 5000 rpm for 10 min.

Synthesis of C-151@ZIF-8^2@F@ZIF-8 (Method B). As-synthesized C-151@ZIF-8^2 was redispersed in 7.0 mL of a solution of 790 mM 2-methylimidazole and 0.41 mM CTAB. The solution was stirred for 5 min, and then 1.0 mL of a 97.5 mM $Zn(NO_3)_2{\cdot}6H_2O$ aqueous solution was added. After the mixture was stirred for 30 s, various amount of 5 mM F solution were added, and the mixture continued to stir for 2 min. Then the solution was left undisturbed for 1 h at room temperature. The synthesized C-151@ZIF-8^2@F@ZIF-8 composites were spun down at 4000 rpm for 10 min and washed twice using methanol.

Synthesis of C-151@ZIF-8^2@F@ZIF-8^2. As-synthesized C-151@ZIF-8^2@F@ZIF-8 was redispersed in 30 mL of a 30 mM 2-methylimidazole methanol solution. After the solution was shaken for 5 s, 30 mL of a 30 mM $Zn(NO_3)_2{\cdot}6H_2O$ methanol solution was added. Then the solution was left undisturbed at room temperature for 1 h, and the formed dye@ZIF-8^2 was spun down at 3500 rpm for 10 min.

RB@ZIF-8^2@F@ZIF-8^2 and RB@ZIF-8^2@C-151@ZIF-8^2 were synthesized using the same method as for the synthesis of C-151@ZIF-8^2@F@ZIF-8^2.

Synthesis of C-151@ZIF-8^2@F@ZIF-8^2@RB@ZIF-8^2. C-151@ZIF-8^2@F@ZIF-8^2@RB@ZIF-8^2 was synthesized using the same method as for the synthesis of C-151@ZIF-8^2@F@ZIF-8^2.

ASSOCIATED CONTENT

Supporting Information

The Supporting Information is available free of charge on the ACS Publications website at DOI: 10.1021/jacs.9b07236.

Fluorescence data, PXRD, CIE chromaticity coordinates, and photographs for the sample dispersed in methanol under daylight and UV light (PDF)

AUTHOR INFORMATION

Corresponding Authors

*frank.tsung@bc.edu

*jingli@rutgers.edu

ORCID

Chia-Kuang Tsung: 0000-0002-9410-565X

DOI: 10.1021/jacs.9b07236
J. Am. Chem. Soc. 2019, 141, 14807−14813

Jing Li: 0000-0001-7792-4322

Notes

The authors declare no competing financial interest.

■ ACKNOWLEDGMENTS

Financial support from the National Science Foundation (grant no. DMR-1507210) is greatly acknowledged. X.-Y.L. acknowledges support from the Hoffmann Institute of Advanced Materials (HIAM), Shenzhen Polytechnic. K.X. acknowledges support from the China Scholarship Council (CSC).

■ REFERENCES

(1) Wang, M.-S.; Guo, S.-P.; Li, Y.; Cai, L.-Z.; Zou, J.-P.; Xu, G.; Zhou, W.-W.; Zheng, F.-K.; Guo, G.-C. A Direct White-Light-Emitting Metal-Organic Framework with Tunable Yellow-to-White Photoluminescence by Variation of Excitation Light. *J. Am. Chem. Soc.* **2009**, *131* (38), 13572−13573.

(2) Cui, Y.; Yue, Y.; Qian, G.; Chen, B. Luminescent functional metal-organic frameworks. *Chem. Rev.* **2012**, *112* (2), 1126−1162.

(3) Cui, Y.; Zhang, J.; He, H.; Qian, G. Photonic functional metal−organic frameworks. *Chem. Soc. Rev.* **2018**, *47* (15), 5740−5785.

(4) Lustig, W. P.; Li, J. Luminescent metal−organic frameworks and coordination polymers as alternative phosphors for energy efficient lighting devices. *Coord. Chem. Rev.* **2018**, *373*, 116−147.

(5) Lustig, W. P.; Mukherjee, S.; Rudd, N. D.; Desai, A. V.; Li, J.; Ghosh, S. K. Metal-organic frameworks: functional luminescent and photonic materials for sensing applications. *Chem. Soc. Rev.* **2017**, *46* (11), 3242−3285.

(6) Gong, Q.; Hu, Z.; Deibert, B. J.; Emge, T. J.; Teat, S. J.; Banerjee, D.; Mussman, B.; Rudd, N. D.; Li, J. Solution processable MOF yellow phosphor with exceptionally high quantum efficiency. *J. Am. Chem. Soc.* **2014**, *136* (48), 16724−16727.

(7) Cornelio, J.; Zhou, T. Y.; Alkas, A.; Telfer, S. G. Systematic Tuning of the Luminescence Output of Multicomponent Metal-Organic Frameworks. *J. Am. Chem. Soc.* **2018**, *140* (45), 15470−15476.

(8) Hu, Z.; Huang, G.; Lustig, W. P.; Wang, F.; Wang, H.; Teat, S. J.; Banerjee, D.; Zhang, D.; Li, J. Achieving exceptionally high luminescence quantum efficiency by immobilizing an AIE molecular chromophore into a metal-organic framework. *Chem. Commun.* **2015**, *51* (15), 3045−3048.

(9) Lustig, W. P.; Wang, F.; Teat, S. J.; Hu, Z.; Gong, Q.; Li, J. Chromophore-Based Luminescent Metal-Organic Frameworks as Lighting Phosphors. *Inorg. Chem.* **2016**, *55* (15), 7250−7256.

(10) Newsome, W. J.; Ayad, S.; Cordova, J.; Reinheimer, E. W.; Campiglia, A. D.; Harper, J. K.; Hanson, K.; Uribe-Romo, F. J. Solid State Multicolor Emission in Substitutional Solid Solutions of Metal−Organic Frameworks. *J. Am. Chem. Soc.* **2019**, *141* (28), 11298−11303.

(11) Sava, D. F.; Rohwer, L. E.; Rodriguez, M. A.; Nenoff, T. M. Intrinsic broad-band white-light emission by a tuned, corrugated metal-organic framework. *J. Am. Chem. Soc.* **2012**, *134* (9), 3983−3986.

(12) Rao, X.; Huang, Q.; Yang, X.; Cui, Y.; Yang, Y.; Wu, C.; Chen, B.; Qian, G. Color tunable and white light emitting Tb^{3+} and Eu^{3+} doped lanthanide metal−organic framework materials. *J. Mater. Chem.* **2012**, *22* (7), 3210−3214.

(13) Zhao, H.; Ni, J.; Zhang, J. J.; Liu, S. Q.; Sun, Y. J.; Zhou, H.; Li, Y. Q.; Duan, C. Y. A trichromatic MOF composite for multidimensional ratiometric luminescent sensing. *Chem. Sci.* **2018**, *9* (11), 2918−2926.

(14) Cui, Y.; Song, T.; Yu, J.; Yang, Y.; Wang, Z.; Qian, G. Dye Encapsulated Metal-Organic Framework for Warm-White LED with High Color-Rendering Index. *Adv. Funct. Mater.* **2015**, *25* (30), 4796−4802.

(15) Wen, Y.; Sheng, T.; Zhu, X.; Zhuo, C.; Su, S.; Li, H.; Hu, S.; Zhu, Q. L.; Wu, X. Introduction of Red-Green-Blue Fluorescent Dyes into a Metal-Organic Framework for Tunable White Light Emission. *Adv. Mater.* **2017**, *29* (37), 1700778.

(16) Chen, Y.; Yu, B.; Cui, Y.; Xu, S.; Gong, J. Core−Shell Structured Cyclodextrin Metal−Organic Frameworks with Hierarchical Dye Encapsulation for Tunable Light Emission. *Chem. Mater.* **2019**, *31* (4), 1289−1295.

(17) Tang, Y.; Xia, T.; Song, T.; Cui, Y.; Yang, Y.; Qian, G. Efficient Energy Transfer within Dyes Encapsulated Metal-Organic Frameworks to Achieve High Performance White Light-Emitting Diodes. *Adv. Opt. Mater.* **2018**, *6* (24), 1800968.

(18) Wang, Z.; Zhu, C.-Y.; Mo, J.-T.; Fu, P.-Y.; Zhao, Y.-W.; Yin, S.-Y.; Jiang, J.-J.; Pan, M.; Su, C.-Y. White-Light Emission from Dual-Way Photon Energy Conversion in a Dye-Encapsulated Metal−Organic Framework. *Angew. Chem., Int. Ed.* **2019**, *58*, 9752−9757.

(19) Sun, C. Y.; Wang, X. L.; Zhang, X.; Qin, C.; Li, P.; Su, Z. M.; Zhu, D. X.; Shan, G. G.; Shao, K. Z.; Wu, H.; Li, J. Efficient and tunable white-light emission of metal-organic frameworks by iridium-complex encapsulation. *Nat. Commun.* **2013**, *4*, 2717.

(20) Wang, Z.; Wang, Z.; Lin, B.; Hu, X.; Wei, Y.; Zhang, C.; An, B.; Wang, C.; Lin, W. Warm-White-Light-Emitting Diode Based on a Dye-Loaded Metal-Organic Framework for Fast White-Light Communication. *ACS Appl. Mater. Interfaces* **2017**, *9* (40), 35253−35259.

(21) Xie, W.; He, W. W.; Du, D. Y.; Li, S. L.; Qin, J. S.; Su, Z. M.; Sun, C. Y.; Lan, Y. Q. A stable Alq3@MOF composite for white-light emission. *Chem. Commun.* **2016**, *52* (16), 3288−3291.

(22) Chen, W.; Zhuang, Y.; Wang, L.; Lv, Y.; Liu, J.; Zhou, T. L.; Xie, R. J. Color-Tunable and High-Efficiency Dye-Encapsulated Metal-Organic Framework Composites Used for Smart White-Light-Emitting Diodes. *ACS Appl. Mater. Interfaces* **2018**, *10* (22), 18910−18917.

(23) Liu, X. Y.; Zhang, F.; Goh, T. W.; Li, Y.; Shao, Y. C.; Luo, L.; Huang, W.; Long, Y. T.; Chou, L. Y.; Tsung, C. K. Using a Multi-Shelled Hollow Metal-Organic Framework as a Host to Switch the Guest-to-Host and Guest-to-Guest Interactions. *Angew. Chem., Int. Ed.* **2018**, *57* (8), 2110−2114.

(24) Xiao, J.-D.; Shang, Q.; Xiong, Y.; Zhang, Q.; Luo, Y.; Yu, S.-H.; Jiang, H.-L. Boosting Photocatalytic Hydrogen Production of a Metal−Organic Framework Decorated with Platinum Nanoparticles: The Platinum Location Matters. *Angew. Chem., Int. Ed.* **2016**, *55* (32), 9389−9393.

(25) Chen, Y.-Z.; Gu, B.; Uchida, T.; Liu, J.; Liu, X.; Ye, B.-J.; Xu, Q.; Jiang, H.-L. Location determination of metal nanoparticles relative to a metal-organic framework. *Nat. Commun.* **2019**, *10* (1), 3462.

(26) Pan, Y.; Heryadi, D.; Zhou, F.; Zhao, L.; Lestari, G.; Su, H.; Lai, Z. Tuning the crystal morphology and size of zeolitic imidazolate framework-8 in aqueous solution by surfactants. *CrystEngComm* **2011**, *13* (23), 6937−6940.

(27) Zhuang, J.; Kuo, C.-H.; Chou, L.-Y.; Liu, D.-Y.; Weerapana, E.; Tsung, C.-K. Optimized Metal−Organic-Framework Nanospheres for Drug Delivery: Evaluation of Small-Molecule Encapsulation. *ACS Nano* **2014**, *8* (3), 2812−2819.

(28) Chou, L. Y.; Hu, P.; Zhuang, J.; Morabito, J. V.; Ng, K. C.; Kao, Y. C.; Wang, S. C.; Shieh, F. K.; Kuo, C. H.; Tsung, C. K. Formation of hollow and mesoporous structures in single-crystalline microcrystals of metal-organic frameworks via double-solvent mediated overgrowth. *Nanoscale* **2015**, *7* (46), 19408−19412.

(29) Fairen-Jimenez, D.; Moggach, S. A.; Wharmby, M. T.; Wright, P. A.; Parsons, S.; Duren, T. Opening the gate: framework flexibility in ZIF-8 explored by experiments and simulations. *J. Am. Chem. Soc.* **2011**, *133* (23), 8900−8902.

(30) Hanczyc, P.; Mikhailovsky, A.; Boyer, D. R.; Sawaya, M. R.; Heeger, A.; Eisenberg, D. Ultrafast Time-Resolved Studies on Fluorescein for Recognition Strands Architecture in Amyloid Fibrils. *J. Phys. Chem. B* **2018**, *122* (1), 8−18.

(31) Morabito, J. V.; Chou, L. Y.; Li, Z.; Manna, C. M.; Petroff, C. A.; Kyada, R. J.; Palomba, J. M.; Byers, J. A.; Tsung, C. K. Molecular

DOI: 10.1021/jacs.9b07236
J. Am. Chem. Soc. 2019, 141, 14807−14813

encapsulation beyond the aperture size limit through dissociative linker exchange in metal-organic framework crystals. *J. Am. Chem. Soc.* **2014**, *136* (36), 12540−12543.
(32) Avci, C.; Imaz, I.; Carne-Sanchez, A.; Pariente, J. A.; Tasios, N.; Perez-Carvajal, J.; Alonso, M. I.; Blanco, A.; Dijkstra, M.; Lopez, C.; Maspoch, D. Self-assembly of polyhedral metal-organic framework particles into three-dimensional ordered superstructures. *Nat. Chem.* **2018**, *10* (1), 78−84.
(33) Thomas, S. W.; Joly, G. D.; Swager, T. M. Chemical Sensors Based on Amplifying Fluorescent Conjugated Polymers. *Chem. Rev.* **2007**, *107* (4), 1339−1386.
(34) Yuan, W. Z.; Lu, P.; Chen, S.; Lam, J. W.; Wang, Z.; Liu, Y.; Kwok, H. S.; Ma, Y.; Tang, B. Z. Changing the behavior of chromophores from aggregation-caused quenching to aggregation-induced emission: development of highly efficient light emitters in the solid state. *Adv. Mater.* **2010**, *22* (19), 2159−2163.
(35) Park, K. S.; Ni, Z.; Cote, A. P.; Choi, J. Y.; Huang, R.; Uribe-Romo, F. J.; Chae, H. K.; O'Keeffe, M.; Yaghi, O. M. Exceptional chemical and thermal stability of zeolitic imidazolate frameworks. *Proc. Natl. Acad. Sci. U. S. A.* **2006**, *103* (27), 10186−10191.

DOI: 10.1021/jacs.9b07236
J. Am. Chem. Soc. 2019, 141, 14807−14813